Epilepsy & Behavior 27 (2013) 22–28

Contents lists available at SciVerse ScienceDirect

Epilepsy & Behavior

journal homepage: www.elsevier.com/locate/yebeh

Texture analysis of magnetic resonance images of patients with juvenile myoclonic epilepsy

Márcia Silva de Oliveira [a,c,*], Luiz Eduardo Betting [b,c], Suzana B. Mory [b,c], Fernando Cendes [b,c], Gabriela Castellano [a,c]

[a] Neurophysics Group, State University of Campinas (Unicamp), Brazil
[b] Department of Neurology, State University of Campinas (Unicamp), Brazil
[c] CInAPCe Program (Cooperação Interinstitucional de Apoio a Pesquisas sobre o Cérebro), São Paulo State, Brazil

ARTICLE INFO

Article history:
Received 17 August 2012
Revised 19 November 2012
Accepted 8 December 2012
Available online 28 January 2013

Keywords:
Juvenile myoclonic epilepsy (JME)
Texture analysis
MR images

ABSTRACT

Background/purpose: Juvenile myoclonic epilepsy (JME) is the most frequent subsyndrome of the idiopathic generalized epilepsies, and experimental investigations support that the thalamus is a key structure in the mechanisms of JME. Texture analysis (TA) is an image processing technique which can be used to characterize images such as MRI.
Objective: The goal of this work was to investigate the thalamus of patients with JME using TA, a quantitative neuroimaging technique.
Methods: Patients and controls were submitted to MRI investigation. Images were acquired in a 2-Tesla scanner. The T1 volumetric sequence was used for thalamic segmentation and extraction of texture parameters. Twenty-four patients with a diagnosis of JME and 20 healthy volunteers were investigated.
Results: Texture analysis revealed differences between the right thalamus of patients and controls.
Conclusions: The present investigation supports the participation of the thalamus in the disease mechanisms of JME. Texture analysis may be a useful tool in the quantitative neuroimaging investigation of the epilepsies and can be important to understand JME.

1. Introduction

Juvenile myoclonic epilepsy (JME) is the most frequent subsyndrome of the idiopathic generalized epilepsies (IGE). Seizure onset occurs in adolescence. Myoclonic seizures occur typically in the morning and are usually associated with sleep deprivation. The electroencephalogram may reveal the typical symmetrical generalized spike-and-wave (GSW) discharges with normal background [1,2]. Magnetic resonance imaging (MRI) is not routinely performed in patients with IGE. However, visual analysis of the MR image usually is normal or minor incidental abnormalities may be observed [3].

Magnetic resonance images are inherently digital, which means that they are formed by an array of pixels (picture elements) which can assume numerical values, usually integers, that represent physical properties (e.g., proton density modulated by T1 relaxation effects, in the case of T1-weighted MR images). These numerical values have a direct relationship to the gray levels, or different luminous intensities, seen in the image. Magnetic resonance images usually have values ranging from 0 to 255 or to 4095, depending on the type of image and on the MR equipment. Given that the human eye is able to discriminate between about 64 gray levels at a time [4], simple visual analysis can miss important information in an MR image. The goal of this work was to perform a computational analysis, known as texture analysis, of MR images of patients with JME and control subjects in order to find out if there are tissue differences between the thalami of these groups, which are not perceived by standard visual analysis.

The cortico-thalamic circuitry is a key neuroanatomical pathway involved in the pathophysiology of JME [5,6]. By using quantitative MRI analysis, previous investigations of the thalamus were able to detect subtle abnormalities in the volume of this structure in patients with IGE [7,8].

Texture analysis has already been validated and applied to several areas of medicine, e.g., characterization of brain tumors [9]; detection of affected areas by ischemic brain stroke [10]; detection of focal cortical dysplasia [11]; breast cancer diagnosis [12]; assessment of osteoporosis [13]; study of Alzheimer's disease [14] and multiple sclerosis [15]; comparison between mild cognitive impairment patients and Alzheimer patients [16]; study of Machado–Joseph disease [17]; and study of hippocampal sclerosis in patients with temporal lobe epilepsy [18]. Particularly, studies performed by our group that applied texture analysis to differentiate between 1) Alzheimer patients, mild cognitive impairment patients, and controls [16] and 2) Machado–Joseph disease patients and controls [17] found that texture parameters related to homogeneity, smoothness, and uniformity of the gray level distribution

* Corresponding author at: Neurophysics Group, State University of Campinas (Unicamp), Brazil. Fax: +55 19 35215512.
E-mail address: marciaso@ifi.unicamp.br (M.S. de Oliveira).

1525-5050
http://dx.doi.org/10.1016/j.yebeh.2012.12.009

were increased in patients compared to those of controls, while texture parameters related to inhomogeneity, variation, and dispersion were decreased. Since, to the best of our knowledge, texture analysis has not yet been used to investigate subtle MRI changes in patients with JME, we sought to verify if this same pattern of increase of homogeneity/uniformity parameters and decrease of inhomogeneity/dispersion parameters would be observed in patients with JME with respect to controls.

2. Methods

2.1. Subjects

Juvenile myoclonic epilepsy diagnosis was performed according to clinical and EEG criteria [1,2]. All patients and one individual who had witnessed a typical seizure were re-interviewed, and the medical records were analyzed. Twenty-four patients with JME (16 women, mean age: 30.00 ± 9.24, range: 19–50) and 20 healthy volunteers (10 women, mean age: 30.55 ± 8.46, range: 22–52) were investigated. The project was approved by the Ethical Research Committee of our institution (University of Campinas — Brazil), and all subjects gave their written informed consent.

2.2. MRI scanning protocol

All MRI data were obtained in a 2-Tesla scanner (GE Elscint Prestige, Haifa, Israel). T1-weighted images with 1 mm isotropic voxels were acquired for all subjects using a spoiled gradient echo sequence with flip angle = 35°, repetition time (TR) = 22 ms, echo time (TE) = 9 ms, matrix = 256 × 220, and field of view (FOV) = 23 × 25 cm^2. These images were used for texture analysis. All the images were submitted for visual analysis by two imaging experts. Patients with abnormalities detected by visual analyses of MRI exams were not included in this study.

2.3. Texture analysis

Texture analysis is an important branch of digital image processing that has found application in several research areas, e.g., geosciences and remote sensing [19,20], food sciences [21], minerals engineering [22], and medical images [23–27]. Although a clear definition of texture does not exist, it can be understood as a group of image properties that relate to our intuitive notions of coarseness, rugosity, smoothness etc. [28]. Several approaches have been developed for extracting texture characteristics from digital images; these may be grouped into four categories [29]: transform-based, model-based, structural, and statistical techniques. Transform approaches comprise all methods based on frequency or scale transforms (such as Fourier or Wavelet); they attempt to describe the image regions using their frequency content (Fourier) or their frequency and scale content (Wavelet). In model-based methods, fractal models are used to describe texture. Structural techniques [28] use sets of primitive shapes to describe an object; they include image texture assessment through mathematical morphology operators [30]. Last, statistical approaches [28] use the pixel gray level distribution to extract texture information from the image and are the most used for medical images analysis [31], which seems reasonable given the irregularity of shapes and variety of texture types found in medical images. In the present work, a statistical approach based on the GLC matrix [28] was used to extract texture parameters from MRI images of patients with JME and control subjects.

The GLC matrix approach is a second order statistics method, i.e., it analyzes texture characteristics in the image based on the gray level distribution of pairs of pixels. The GLC matrix is an N × N matrix, where N is the total number of gray levels in the image. Each element (i, j) of this matrix reports how many times gray level i co-occurs with gray level j, given the distance d (usually $d = 1, 2, 3, 4$ or 5 pixels) and the direction θ ($\theta = 0°$, 45°, 90° or 135°) between the corresponding pixel pair. Fig. 1 shows an example of a 4 × 4 digital image with 4 gray levels (0 to 3) and corresponding GLC matrices for $d = 1$ in the horizontal direction (Fig. 1c) and $d = 1$ in a diagonal direction (Fig. 1d).

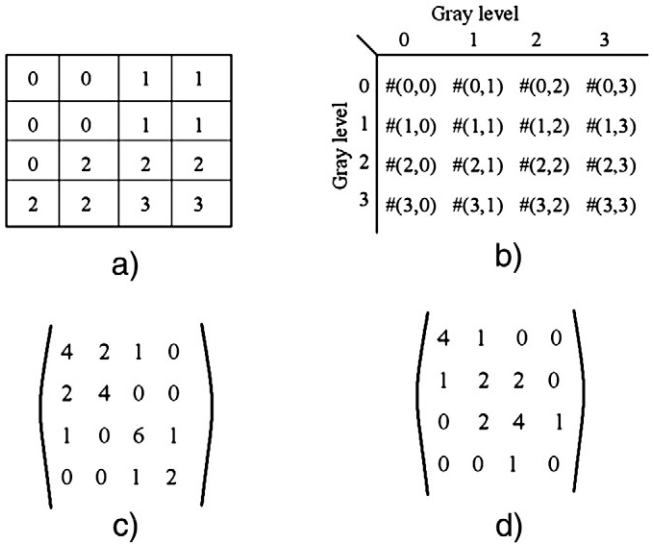

Fig. 1. An example of a GLC matrix. (a) An image with gray levels between 0 and 3. (b) Standard form of a GLC matrix. (c) GLC matrix for image in (a) with $d = 1$ and $\theta = 0°$. (d) GLC matrix for image in (a) with $d = 1$ and $\theta = 45°$.
Adapted from [28].

After computing the GLC matrix, the image can be analyzed according to Haralick's texture descriptors [28], which are computed from the matrix. Materka reported the use of 11 descriptors [29] which were chosen for use in this work: Angular Second Moment

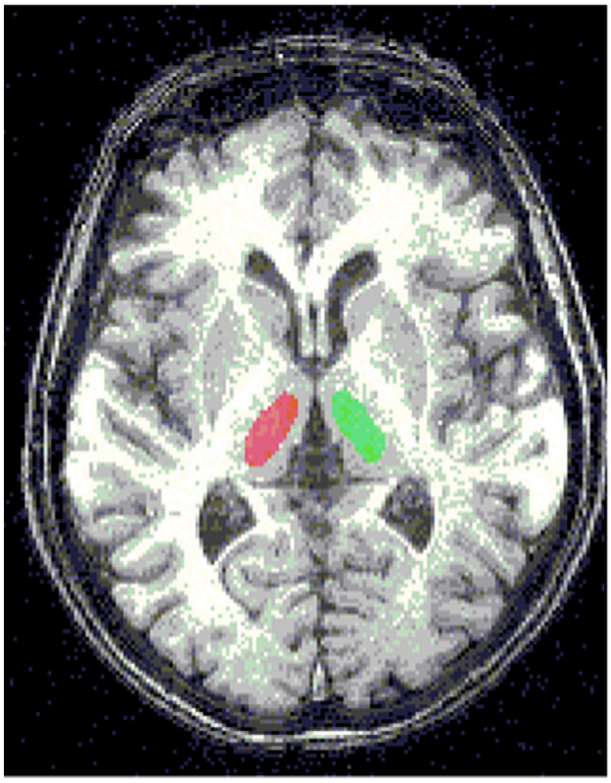

Fig. 2. Segmentation of the thalamus for textural analysis (control).

Table 1
Significant texture parameters obtained for the right thalamus in the comparison between patients with JME and controls.

Distance (d)	Texture parameter	Mean ± SD (cont)	Mean ± SD (pat)	p-Value
3	Contrast	22.746 ± 2.607	25.078 ± 3.244	0.014
3	Inverse Difference Moment	0.227 ± 0.013	0.218 ± 0.013	0.043
3	Difference Variance	8.154 ± 0.900	8.962 ± 1.159	0.017
3	Difference Entropy	0.987 ± 0.023	1.004 ± 0.024	0.013
4	Contrast	27.264 ± 3.127	30.192 ± 4.200	0.022
4	Difference Variance	9.351 ± 1.108	10.307 ± 1.390	0.013
4	Difference Entropy	1.013 ± 0.024	1.029 ± 0.025	0.040
5	Sum of Squares	15.103 ± 2.225	16.396 ± 2.501	0.048

(ASM), Contrast (CT), Correlation (CO), Sum of Squares (SS), Inverse Difference Moment (IDM), Sum Averages (SA), Sum Variances (SV), Sum Entropy (SE), Entropy (E), Difference Variance (DV), and Difference Entropy (DE).

In Table 2, we present the formulae and description for the texture parameters used in this work.

2.4. Image processing

The images were analyzed with the *MaZda* program [32], which was used to segment the thalami (left and right) for texture analysis. This program only allows manual (mouse delineated) segmentation. However, this is acceptable, since the chosen structure is easily discernible in the images. Therefore, segmentation was based on anatomical criteria, with the assumption that texture in these structures should be approximately constant along the structure. All segmentations were checked by an expert neurologist. The thalamus was segmented into seven consecutive slices: the central slice (determined by the *MRIcro* program — www.mccauslandcenter.sc.edu/mricro), three to the right, and three to the left in the axial view (Fig. 2). After segmentation, texture analysis was performed for each segmented region of interest (ROI) in the selected slices, also using the *MaZda* program. This was accomplished by computing the gray level co-occurrence (GLC) matrices for the default *MaZda* distances (1 to 5 pixels) and directions ($\theta = 0°$, 45°, 90°, or 135°), totalling 20 GLC matrices for every ROI. From these matrices, 11 texture descriptors (see Section "Texture analysis") were calculated for use in the analysis, totalling 220 texture parameters for each ROI (for each slice).

A weighted average over slices (using the ROI size, or number of pixels in the ROI, in each slice, as weight) was then computed for each of the 220 texture parameters, using *Matlab* (www.mathworks.com). This resulted in a single set of texture parameters for each thalamus (left or right) for every subject. This set of parameters was further used to calculate an average over the different GLC directions (giving 55 parameters for each thalamus), since it is expected that textures should be approximately isotropic (and otherwise, the positioning of the patient's head should not influence the texture measurement). These parameter sets (55 parameters for each thalamus) were used in the statistical analysis performed with the *Systat 10.2* software (www.systat.com). The statistical test used was the nonparametric Mann–Whitney test [33]. Receiver operating characteristic

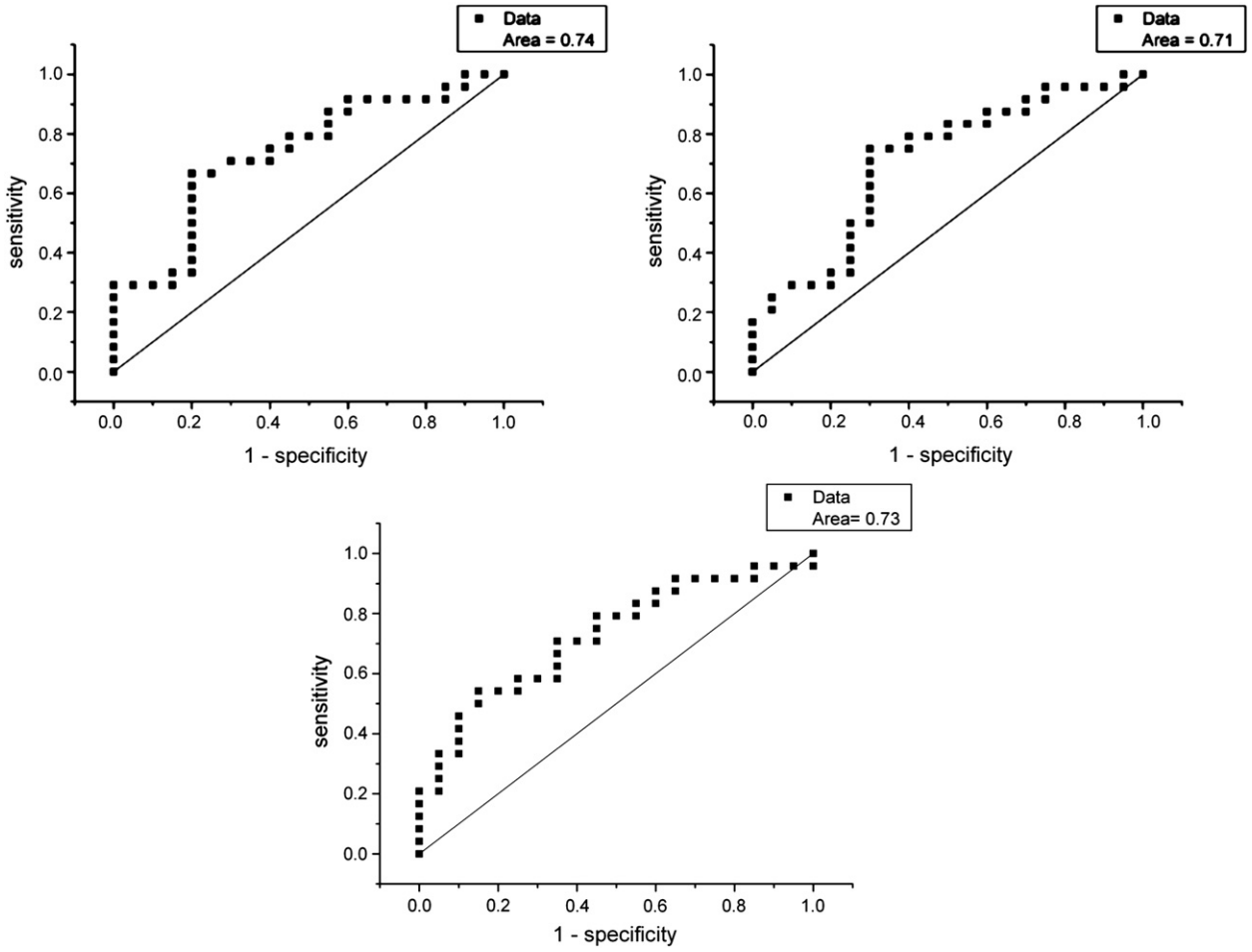

Fig. 3. ROC curves for a) Contrast ($d = 3$), b) Difference Variance ($d = 3$), c) Difference Entropy ($d = 4$).

(ROC) curves for the statistically significant parameters were also calculated. Corrections for multiple comparisons were not made due to the exploratory nature of this study.

3. Results

The statistical analysis showed differences between the texture parameters of patients with JME and controls only for the right thalamus. The differences in texture came from the parameters computed from the GLC matrices for distances of 3 to 5 pixels. Table 1 shows the statistically significant ($p<0.05$) results obtained, giving the GLC matrix distance, the texture parameter, its mean value for each group, and the corresponding p-value. Differences between patients and controls were found for distances $d=3$, 4, and 5. Particularly, for distances $d=3$ and $d=4$, three significant texture parameters were the same: Contrast ($p<0.015$ and $p<0.025$, for $d=3$ and $d=4$, respectively), Difference Variance ($p<0.02$ and $p<0.015$, respectively), and Difference Entropy ($p<0.015$ and $p<0.005$, respectively). All these parameters showed an increase for the patient group compared to those for the controls. For distance $d=3$, the parameter Inverse Difference Moment was also significant ($p<0.05$), showing a decrease for the patients' group. Finally, for distance $d=5$, the parameter Sum of Squares was also significant ($p<0.05$), showing again an increase for patients.

To illustrate the difference in texture parameters between the patient and control groups, Fig. 3 shows maps of two texture parameters, namely Contrast (second row) and Difference Variance (third row) for one control and two patients. These maps were calculated for a GLC distance $d=4$ pixels and direction $\theta=45°$. In both patients, brighter areas can be seen in the thalamus when compared to the control. It is important to note that differences also appear in other patients and directions. However, as previously mentioned, the final texture parameters used in the statistical tests did not take into account the direction of the GLC matrices, since an average over the different directions was taken for the texture parameters in order to avoid influence of the head positioning in the images.

In order to assess the sensibility and specificity of these parameters for differentiating among the groups, ROC curves were computed for the parameters that gave the best differentiation (smallest p-value). These are shown in Fig. 3 for Contrast and Difference Variance ($d=3$) and for Difference Entropy ($d=4$).

4. Discussion

In this work, we sought to differentiate patients with JME from healthy controls, using texture analysis of the T1-MR images of the thalami of these subjects. Indeed, this analysis was able to detect differences between the thalami of patients with JME and controls. Some of the texture parameters used have an intuitive meaning (as described in Table 2), while others are just mathematical definitions, and they are a form of characterizing the gray level distributions of each analyzed ROI. These gray level distributions, in turn, underlie physical properties regarding the imaged tissues. In this work, the corresponding physical property is the T1-weighted MR signal.

Table 1 shows that the parameters that differentiated among the JME and control groups were Contrast, Difference Variance, Difference Entropy, Sum of Squares, and Inverse Difference Moment. From this table, we can see that with exception of the Inverse Difference Moment, all parameter values are higher for the patients. Indeed, parameters such as Contrast, Difference Variance, Difference

Table 2
Formulae and description for texture parameters used in this work.

Texture parameter	Formula[a]	Description
Angular Second Moment (Energy, Uniformity)	$\sum_{i=1}^{N_g}\sum_{j=1}^{N_g} p(i,j)^2$	Measures the uniformity (or orderliness) of the gray level distribution of the image; images with smaller number of gray levels have larger Uniformity
Contrast	$\sum_{n=0}^{N_g-1}(i-j)^2\left\{\sum_{i=1}^{N_g}\sum_{j=1}^{N_g} p(i,j)\right\}$	Represents the amount of local gray level variation in an image; a high value of this parameter may indicate the presence of edges, noise, or "wrinkled" textures in the image
Correlation	$\sum_{i=1}^{N_g}\sum_{j=1}^{N_g}\frac{(ij)p(i,j)-\mu_x\mu_y}{\sigma_x\sigma_y}$	Measures the linear dependency of gray levels on those of neighboring pixels; it provides a measure similar to autocorrelation methods
Sum of Squares (Variance)	$\sum_{i=1}^{N_g}\sum_{j=1}^{N_g}(i-\mu)^2 p(i,j)$	Measures the dispersion (with regard to the mean) of the gray level distribution
Inverse Difference Moment (Homogeneity)	$\sum_{i=1}^{N_g}\sum_{j=1}^{N_g}\frac{p(i,j)}{1+(i-j)^2}$	Measures the smoothness (homogeneity) of the gray level distribution of the image; it is (approximately) inversely correlated with Contrast — if the Contrast is small, the IDM is large
Entropy	$-\sum_{i=1}^{N_g}\sum_{j=1}^{N_g} p(i,j)\log(p(i,j))$	Measures the degree of disorder among pixels in the image; it is (approximately) inversely correlated with Angular Second Moment; images with larger number of gray levels have larger Entropy
Sum Average[b]	$\sum_{i=2}^{2N_g} i p_{x+y}(i)$	Measures the mean of the sum gray level distribution of the image
Sum Variance[b]	$\sum_{i=2}^{2N_g}\left(i-\left[\sum_{i=2}^{2N_g} i p_{x+y}(i)\right]\right)^2$	Measures the dispersion (with regard to the mean) of the sum gray level distribution of the image
Sum Entropy[b]	$-\sum_{i=2}^{2N_g} p_{x+y}(i)\log\left\{p_{x+y}(i)\right\}$	Measures the disorder related to the sum gray level distribution of the image
Difference Variance[c]	$\sum_{i=2}^{2N_g}\left(i-\left[\sum_{i=2}^{2N_g} i p_{x-y}(i)\right]\right)^2$	Measures the dispersion (with regard to the mean) of the difference gray level distribution of the image
Difference Entropy[c]	$-\sum_{i=0}^{N_g-1} p_{x-y}(i)\log\left\{p_{x-y}(i)\right\}$	Measures the disorder related to the difference gray level distribution of the image

[a] In all equations, $p(i,j)$ is the (i,j)-th entry of the normalized GLC matrices, i.e., $p(i,j)=P(i,j)/\sum_{ij}P(i,j)$, where $P(i,j)$ is the (i,j)-th entry of the computed GLC matrices, and N_g is the total number of gray levels in the image.

[b] The sum gray level distribution is given by $p_{x+y}(k)=\sum_{\substack{i=1\\ i+j=k}}^{N_g}\sum_{j=1}^{N_g} p(i,j)$, $k=2, 3\ldots, 2N_g$; it is related to the distribution of the sum of adjacent (co-occurrent) pixels in the image.

[c] The difference gray level distribution is given by $p_{x-y}(k)=\sum_{\substack{i=1\\ |i-j|=k}}^{N_g}\sum_{j=1}^{N_g} p(i,j)$, $k=0, 1, 2\ldots, N_g-1$; it is related to the distribution of the difference between adjacent (co-occurrent) pixels in the image.

Entropy, and Sum of Squares represent properties such as high variability, or low uniformity, while the Inverse Difference Moment parameter (also called Homogeneity) represents exactly the opposite. Therefore, we see that these parameters indicate, somehow, an increase in variability, or decrease in uniformity, of the underlying thalamic tissue in patients with JME compared to controls.

This observation supports the concept of a subtle structural abnormality in the thalamus that may be related to the underlying pathophysiology of JME. The thalamic functionality is complex and not completely understood. Ventral anterior, ventral lateral, and mediodorsal nuclei apparently are responsible to relay basal ganglia output within specific cortical circuits. These nuclei also may mediate the information flow between cortical circuits [34]. The connections of the cortex and the thalamus are extensive including projections to the motor areas (primary, supplementary, and premotor) [34]. These networks are involved in several cortical functions including the modulation of the wake–sleep cycle. Probably, a failure in this mechanism is the key for generation of the GSW discharges [35]. The present investigation disclosed a thalamic abnormality that supports a disruption in this system. Other investigations using diffusion tensor imaging are

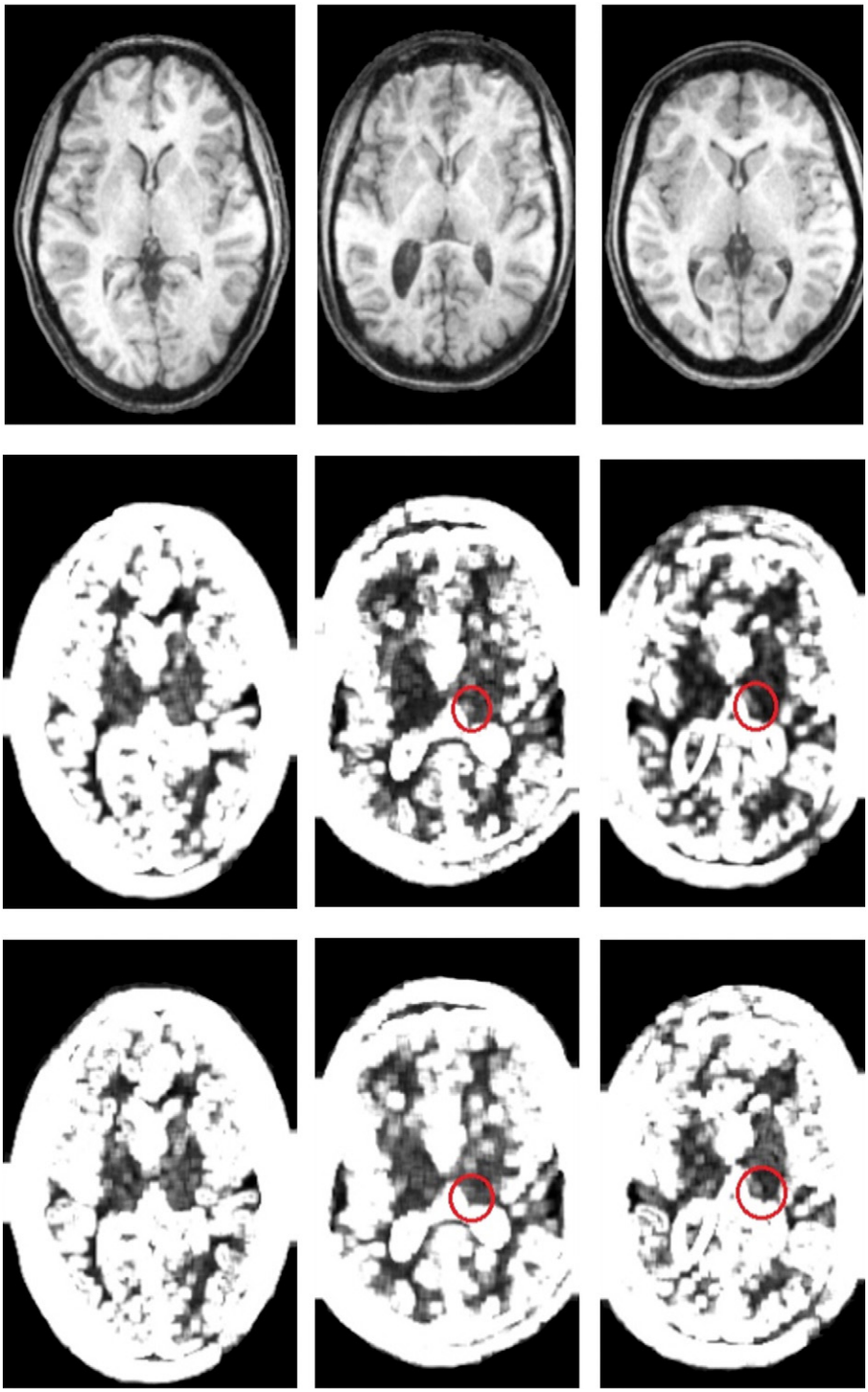

Fig. 4. First row: MRI of one control (left) and two patients (middle and right). Second row: corresponding Contrast maps. Third row: corresponding Difference Variance maps. In all cases $d = 4$, $\theta = 45°$. Images are displayed in the axial orientation and in the neurological convention (right on right).

also in line with this hypothesis showing reduced white matter connectivity of the supplementary motor area in patients with JME [36].

Previous neuropathology investigations did not demonstrate neuronal loss in the thalamus of patients with JME [37]. Moreover, a volumetric study conducted in the thalamus of patients with JME showed increased anterior thalamic volumes in patients with JME with absence seizures [38]. The abnormalities observed in the texture analysis performed here may be more closely related to axonal and neurotransmitters changes. This hypothesis is in line with the genetic profile described in some families with IGE and with previous investigations using quantitative MRI and magnetic resonance spectroscopy [39,40].

To assess whether texture parameters could be used for classifying new cases, ROC curves were computed for the best discriminating parameters, which are shown in Fig. 4. The area under the curve (AUC) calculated for these curves was 0.74 for Contrast (calculated for the GLC distance $d=3$), 0.71 for Difference Variance ($d=3$), and 0.73 for Difference Entropy ($d=4$). The AUC represents the probability that a randomly selected patient will have a higher test result (in this case, texture parameter value) than a randomly selected control, where AUC = 0.5 corresponds to a non-informative test and AUC = 1 corresponds to the perfect test [41]. Also, according to Swets [41], an AUC in the interval [0.7–0.9] could be regarded as a "highly accurate" test, which is the case of the results obtained with these parameters, while a result below this interval would be "moderately accurate". Nevertheless, AUC values below 1.0 mean that there is no cutoff value for the corresponding parameter that will completely differentiate between patients and controls. However, some combination of these texture parameters might be able to perform this separation, and we have already started a study regarding this issue.

Although by definition, visual analysis of the MRI in JME appears normal [1], the texture parameter maps shown in Fig. 3 (Contrast and Difference Variance) corroborate the fact that there are indeed subtle differences between the MRI images of patients with JME and controls, but that these differences surface only upon numerical processing of the images. These maps were obtained by selecting a small neighborhood (9×9 pixels) around each image pixel, computing the texture parameter for that neighborhood, and then attributing the value of this parameter to the pixel. This was done for all brain pixels and not just in the region of interest. Obviously, this is different from calculating these parameters for the segmented ROIs, which are not rectangular and are much larger in size (the thalamus ROIs have approximately 120–150 pixels, against the 81 pixels of the considered neighborhoods for the maps calculations). Nevertheless, these maps give an idea about the texture variation in the brain, and they "visually" show that there are, indeed, texture differences of the right thalamus between JME and control individuals.

Furthermore, only abnormalities in the right thalamus were observed in the group analysis, although when performing analyses in individual patients, some of them presented bilateral abnormalities as illustrated in Fig. 3. These findings may be related with the heterogeneity observed in the IGE phenotype. Therefore, further investigations of this structure in patients with JME are needed.

5. Conclusions

Our results demonstrate abnormal MRI texture in the thalamus of patients with JME undetected by visual analyses. Texture analysis has potential to become a helpful tool in the investigation of subtle abnormalities in patients with JME.

Acknowledgments

We thank CNPq-Brazil for the financial support and Dr. João Ricardo Sato for the statistical support.

References

[1] Commission on classification and terminology of the International League Against Epilepsy. Proposal for revised classification of epilepsy and epileptic syndromes. Epilepsia 1989;30:389–99.
[2] Panayiotopoulos CP. Idiopathic generalized epilepsies. In: Panayiotopoulos CP, editor. A clinical guide to epileptic syndromes and their treatment. Oxfordshire (UK): Bladon Medical Publishing; 2002. p. 115–60.
[3] Betting LE, Mory SB, Lopes-Cendes I, et al. MRI reveals structural abnormalities in patients with idiopathic generalized epilepsy. Neurology 2006;67:848–52.
[4] Voigt H. The 'digital eye' at the threshold of cancer diagnosis. Expert Rev Anticancer Ther 2002;2(5):478–9.
[5] Gloor P. Generalized epilepsy with spike-and-wave discharge: a reinterpretation of its electrographic and clinical manifestations. Epilepsia 1979;20:571–88.
[6] Meeren HK, Pijn JP, Van Luijtelaar EL, et al. Cortical focus drives widespread corticothalamic networks during spontaneous absence seizures in rats. J Neurosci 2002;22:1480–95.
[7] Betting LE, Mory SB, Lopes-Cendes I, et al. Voxel-based morphometry in patients with idiopathic generalizes epilepsies. Neuroimage 2006;32:498–502.
[8] Chan CH, Briellmann RS, Pell GS, et al. Thalamic atrophy in childhood absence epilepsy. Epilepsia 2006;47:399–405.
[9] Georgiadis P, Cavouras D, Kalatzis I, et al. Enhancing the discrimination accuracy between metastases, gliomas and meningiomas on brain MRI by volumetric textural features and ensemble pattern recognition methods. Magn Reson Imaging 2009;27:120–30.
[10] Oliveira MS, Fernandes PT, Avelar WM, et al. Texture analysis of computed tomography images of acute ischemic stroke patients. Braz J Med Biol Res 2009;42:1076–9.
[11] Besson P, Bernasconi N, Colliot O, et al. Surface-based texture and morphological analysis detects subtle cortical dysplasia. Med Image Comput Comput Assist Interv 2008;11(Pt 1):645–52.
[12] McLaren C, Chen W, Nie K, et al. Prediction of malignant breast lesions from MRI features: a comparison of artificial network and logistic regression techniques. Acad Radiol 2009;16:842–52.
[13] Rachidi M, Breban S, Benhamou CL. The challenges of the bone microarchitecture. J Soc Biol 2008;202(4):265–73.
[14] Kaeriyama T, Kodama N, Shimada T, et al. Application of run-length matrix to magnetic resonance imaging diagnosis of Alzheimer-type dementia. Nippon Hoshasen Gijutsu Gakkai Zasshi 2002;58(11):1502–8.
[15] Theocharakis P, Glotsos D, Kalatzis I, et al. Pattern recognition system for the discrimination of multiple sclerosis from cerebral microangiopathy lesions based on texture analysis of magnetic resonance images. Magn Reson Imaging 2009;27:417–22.
[16] Oliveira MS, Balthazar MLF, D'Abreu A, et al. MRI texture analysis of corpus callosum and thalamus in amnestic mild cognitive impairment and mild Alzheimer's disease. Am J Neuroradiol 2011;32:60–6.
[17] Oliveira MS, D' Abreu A, França Jr MC, et al. MRI-texture analysis of corpus callosum, thalamus, putamen and caudate in Machado–Joseph disease. J Neuroimaging 2012;22(1):46–52.
[18] Bonilha L, Kobayashi E, Castellano G, et al. Texture analysis of hippocampal sclerosis. Epilepsia 2003;44:1546–50.
[19] Nagai M, Chen T, Shibasaki R, et al. UAV-borne 3-D mapping system by multisensor integration. IEEE Trans Geosci Remote Sens 2009;47(3):701–8.
[20] Laliberte AS, Rango A. Texture and scale in object-based analysis of subdecimeter resolution unmanned aerial vehicle (UAV) imagery. IEEE Trans Geosci Remote Sens 2009;47(3):761–70.
[21] Zheng CX, Sun DW, Zheng LY. Recent applications of image texture for evaluation of food qualities — a review. Trends Food Sci Technol 2006;17(3):113–28.
[22] Bartolacci G, Pelletier P, Tessier J, et al. Application of numerical image analysis to process diagnosis and physical parameter measurement in mineral processes — part I: flotation control based on froth textural characteristics. Miner Eng 2006;19(6–8):734–47.
[23] Giger ML, Chan HP, Boone J. Anniversary paper: history and status of CAD and quantitative image analysis: the role of medical physics and AAPM. Med Phys 2008;35(12):5799–820.
[24] Maglogiannis I, Kosmopoulos DI. Computational vision systems for the detection of malignant melanoma. Oncol Rep 2006;15(SI):1027–32.
[25] Kazakia GJ, Majumdar S. New imaging technologies in the diagnosis of osteoporosis. Rev Endocr Metab Disord 2006;7(1–2):67–74.
[26] Pizurica A, Wink AM, Vansteenkiste E, et al. A review of wavelet denoising in MRI and ultrasound brain imaging. Curr Med Imaging Rev 2006;2(2):247–60.
[27] Lespessailles E, Chappard C, Bonnet N, et al. Imaging techniques for evaluating bone microarchitecture. Joint Bone Spine 2006;73(3):254–61.
[28] Haralick RM. Statistical and structural approaches to texture. Proc IEEE 1979;67:788–804.
[29] Materka A, Strzelecki M, et al. Texture analysis methods — a review. Technical University of Lodz, Institute of Electronics, COST B11 Report, Brussels; 1998.
[30] Dougherty ER, Lotufo RA. Hands-on morphological image processing. Bellingham — WA: SPIE Press; 2003.
[31] Castellano G, Bonilha L, Li LM, Cendes F, et al. Texture analysis in medical images. Clin Radiol 2004;59(12):1061–9.
[32] Szczypiński PM, Strzelecki M, Materka A, et al. MaZda — a software package for image texture analysis. Comput Methods Programs Biomed 2009;94:66–76.
[33] Witte and Witte. Statistics. 6th edition. Hoboken, NJ: John Wiley & Sons. Inc.; 2001. p. 358–60.

[34] McFarland NR, Haber SN. Thalamic relay nuclei of the basal ganglia form both reciprocal and nonreciprocal cortical connections, linking multiple frontal cortical areas. J Neurosci 2002;22:8117–32.
[35] Chang BS, Lowenstein DH. Mechanism of disease: epilepsy. N Engl J Med 2003;349:1257–66.
[36] Vulliemoz S, Vollmar C, Koepp MJ, et al. Connectivity of the supplementary motor area in juvenile myoclonic epilepsy and frontal lobe epilepsy. Epilepsia 2011;52(3):507–14.
[37] Meencke HJ, Janz D. Neuropathological findings in primary generalized epilepsy: a study of eight cases. Epilepsia 1984;25:8–21.
[38] Betting LE, Mory SB, Lopes-Cendes I, et al. MRI volumetry shows increased anterior thalamic volumes in patients with absence seizures. Epilepsy Behav 2006;8(3):575–80.
[39] Helbig I, Scheffer IE, Mulley JC, et al. Navigating the channels and beyond: unraveling the genetics of the epilepsies. Lancet Neurol 2008;7:231–45.
[40] Mory SB, Li LM, Guerreiro CA, et al. Thalamic dysfunction in juvenile myoclonic epilepsy: a proton MRS study. Epilepsia 2003;44:1402–5.
[41] Swets JA. Measuring the accuracy of diagnostic systems. Science 1988;240:1285–93.